International Journal of Pharmaceutics 671 (2025) 125288

Contents lists available at ScienceDirect

International Journal of Pharmaceutics

journal homepage: www.elsevier.com/locate/ijpharm

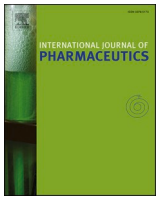

Investigation of aerosol jet printing for the preparation of solid dosage forms

Alice J. Turner [a,*], Elke Prasad [a,b], Alastair J. Florence [a], Gavin W. Halbert [a,b]

[a] EPSRC CMAC Future Manufacturing Research Hub, Strathclyde Institute of Pharmacy and Biomedical Sciences, University of Strathclyde, 99 George Street, Glasgow G1 1RD UK
[b] The Cancer Research UK Formulation Unit, Strathclyde Institute of Pharmacy and Biomedical Sciences, University of Strathclyde, 161 Cathedral St, Glasgow G4 0RE UK

ARTICLE INFO

Keywords:
Aerosol jet printing
Solubility
Additive manufacturing
Personalised medicine
Solid dispersion
Amorphous
Scalability

ABSTRACT

Oral drug delivery remains the preferred method of drug administration but due to poor solubility many active pharmaceutical ingredients (APIs) are ill suited to this. A number of methods to improve solubility of poorly soluble Biopharmaceutical Classification System (BCS) Class II drugs already exist but there is a lack of scalable, flexible methods. As such the current study applies the innovative technique of aerosol jet printing to increase the dissolution capabilities of a Class II drug in a manner which permits flexibility to allow dosage form tailoring. Aerosol jet printing provided a high degree of control allowing effective scaling, by size and layering, and control over drug distribution. Aerosol jet printing of pure active pharmaceutical ingredient (fenofibrate) resulted in crystalline material but as polymer excipient content was increased, morphological changes occurred and a fully amorphous product was generated on inclusion of 75 % (w/w solute) polymer content or above. This amorphous product has been found to exhibit a 10-fold increase in drug dissolution relative to comparable physical mixtures. In conclusion, aerosol jet printing is a novel and effective, scalable method providing improved dissolution coupled with high spatial precision and warrants further investigation.

1. Introduction

Aerosol jet printing is a novel form of inkjet printing. Inkjet printing has been investigated as a method for dosage form production in recent years due to its potential in personalised medicine and possible higher degree of precision than some conventional manufacturing methods (Carou-Senra et al., 2024). Inkjet printing is a broad description for a range of methods for the digitally controlled formation and deposition of small droplets onto a surface (Daly et al., 2015). This can take the form of a liquid binder applied to a powder bed consisting of drug and excipient to cause particle adhesion. Equally, it can consist of an “ink” formulation, either suspension or solution consisting of drug and excipient, being applied to a suitable substrate such as acetate or rice paper in a similar manner to conventional ink printing on paper (Daly et al., 2015; Yun et al., 2009). Inkjet printing can also be used as an additive manufacturing technique, building up dosage forms in a mould-less fashion by layering slices of material (Yun et al., 2009). This allows a degree of flexibility as the dosage form can be built up from polymer alone, drug alone, pre-formulated layers or from a combination of the two (Wickström et al., 2015).

From a solid state perspective, it has been demonstrated previously that inkjet printing can result in formation of amorphous products. With amorphous forms generally possessing higher kinetic solubility than their crystalline forms, with possible increases of 1.1 to 1000 fold (Aoki et al., 2021; Danda et al., 2019; Kawabata et al., 2011; Uchiyama et al., 2021), this is highly favourable for processing of Biopharmaceutical Classification System (BCS) class II and IV drugs. Wickström et al. reported that the amorphous form of indomethacin could be generated by inkjet printing, even in the absence of a stabilising polymer, leading to greater overall dissolution (Wickström et al., 2015). Likewise, greater kinetic solubility was generated by forming an amorphous form of felodipine in another study by Scoutaris et al. (Scoutaris et al., 2011). However, both studies conceded a need for greater solid state investigation.

Whilst inkjet printing offers significant advantages in terms of precision, flexibility and solid state transition, manufacturing aspects such as nozzle size, substrate options, drying time and spatial resolution are limited (Carou-Senra et al., 2024). Thus, there is significant scope for

* Corresponding author.
E-mail address: alice.j.turner@strath.ac.uk (A.J. Turner).

https://doi.org/10.1016/j.ijpharm.2025.125288
Received 26 November 2024; Received in revised form 15 January 2025; Accepted 26 January 2025
Available online 27 January 2025

development in the printed formulation space and this may be fulfilled by novel technique of aerosol jet printing.

An aerosol jet printer functions by passing pressurised nitrogen through ink to cause pneumatic atomisation, forming small droplets which are then propelled through a virtual impactor, extracting any excess nitrogen to condense the stream before traversing the tubing and then condensing further to form a usable stream at the print head (Wilkinson et al., 2019). Aerosol jet printing can be thought of as a miniaturised version of spray drying as the use of volatile solvent in combination with atomisation results in formation of microdroplets followed by rapid drying of particles (Hyun et al., 2015).

Research with this particular type of printer has been based around multiple applications mainly in electronics often using conductive silver ink (Abt et al., 2018; Gramlich et al., 2023), for example, the production of stretchable electronics with silicon (Goh et al., 2018), conformal printing (Goh et al., 2022; Niu et al., 2024), micropillar arrays (Ali et al., 2022), metal inks in 3D chip interconnects (Lan et al., 2017), nano-thermites for antennas (Gamba et al., 2023), sensors on non-planar surfaces (Pavec et al., 2018), multi-dimensional sensors (Zhou et al., 2023), batteries (Deiner et al., 2019; Lopez-Hallman et al., 2024), fuel cells, and supercapacitors (Deiner et al., 2019), high resolution conductive platinum microstructures (Arsenov et al., 2021), transparent conductive silver nanowire electrodes (Serbest et al., 2024), wearable electromyographic sensors (Perilli et al., 2024), gold and indium oxide sensors for simultaneous detection of temperature and strain (Bappy et al., 2024a; Bappy et al., 2024b), graphene channels (Pandhi et al., 2018), and polymer solar cells (Yang et al., 2011). It has also been applied to biological solutions such as proteins and silk (Williams et al., 2020; Xiao et al., 2020) and a range of applications with polymers (Ako et al., 2023; Davies et al., 2024; De Silva et al., 2006; Monne et al., 2021; Overmeyer et al., 2019; Taccola et al., 2024; Tait et al., 2015, Zhang et al., 2024).

Although aerosol jet technology has not been applied previously in pharmaceutical manufacturing, this previous work has demonstrated numerous technological advantages over standard inkjet printing that may be applicable in pharmaceutical systems:

1.1. Improved material deposition

Aerosol jet printing holds significant benefits over standard inkjet printing techniques as it is contactless and thus eliminates the sweeping and tugging actions normal inkjet printers exhibit, aiming to reduce the chance of accidental removal of the previous surface on the application of a new surface (Buanz et al., 2011).

1.2. Substrate flexibility

The contactless nature of the printer also offers the advantage that different substrates may be used as they do not have to pass through a printer mechanism.

1.3. Improved manufacturing efficiency

Unlike conventional inkjet printing, it also dries more quickly allowing a fresh layer to be added more efficiently (Werner et al., 2013), potentially leading to faster manufacturing times.

1.4. Higher spatial resolution and nozzle size options

It may also allow significantly narrower deposition lines to be achieved compared with conventional inkjet printing as the more focused nozzle stream allows greater control (Feng et al., 2021; Seifert et al., 2015; Werner et al., 2013).

As this type of aerosol jet printer offers advantages over inkjet printing and has never previously been applied in pharmaceutical manufacturing, the current study aimed to investigate the application of aerosol jet printing to the production of solid oral dosage forms with a view to determining the capabilities and limitations of the technique. Printer capabilities were tested by programming different output shapes and sizes, along with nozzle size and different substrates, enabling potential in the personalised medicine field. Printed systems were tested for content and physical characteristics including dissolution. The model biopharmaceutical classification system Class II drug fenofibrate was utilised due to its very poor aqueous solubility and proven increase in dissolution capability on solid dispersion formation by prior means such as thin film freezing (Zhang et al., 2012) and hot melt extrusion (Kallakunta et al., 2020). This new technique may offer benefits over these prior techniques as it does not require application of heat or cooling, and thus may allow a greater range of Class II APIs to be formulated in the future.

2. Materials and methods

2.1. Materials

Fenofibrate and phosphoric acid were obtained from Sigma-Aldrich (Dorset, UK). Polyvinylpyrrolidone K30 (PVP K30) was obtained from Sigma-Aldrich (Dorset, UK) and BASF (Ludwigshafen, Germany). Sodium hydroxide and potassium dihydrogen phosphate were obtained from Merck Millipore (Burlington, MA, USA). Ethanol (ABS) and acetonitrile were obtained from VWR International (Lutterworth, U.K.) and Honeywell International (Bucharest, Romania). Rice paper was obtained from Easy Bake (U.K.). Deionised water was produced using a Merck Millipore purification system (Watford, U.K.).

2.2. Methods

2.2.1. Ink rheology

Inks were measured using a Thermoscientific Haake Mars Liquid Rheometer with a double cone DC60/1°TiL and a TMP60DC lower plate using Haake Rheowin Job Manager, over a range of 0–1000 s^{-1} shear taking incremental measurements at 25 °C. Data was analysed using Haake Rheowin Data manager.

2.2.2. Dosage form manufacture by aerosol jet printing

Ink was prepared by dissolving either fenofibrate alone or with PVP K30 in ethanol to achieve a solution viscosity of less than 1000 cP as required by the aerosol jet printer. The inks were prepared with a fenofibrate concentration of 30 mg/ml as standard and a varying concentration of polymer: 0, 15, 30, 45, 60, 90 and 120 mg/ml (Table 1).

Aerosol jet printing was performed using an Optomec Aerosol Jet® 200 3D Inkjet Printer (Optomec Ltd., Albuquerque, U.S.A). The chosen ink solution was loaded into the pneumatic atomiser and atomised to a vapour capable of traversing the tubing and the deposition head. Pneumatic atomisation was achieved by applying nitrogen to the printer at 90 psi, lowering this to 45 psi within the printer and using this pressurised nitrogen to vaporise the ink. A bubbler was not used due to the lack of control over solvent content. The Optomec program KEWA Process Control 2.5.6 was used to control the pressure entering the atomiser, tubing and deposition head by setting the sheath flow rate to

Table 1
Ink Solute Components.

Polymer content (%, w/w solute)	API concentration (mg/mL)	Polymer concentration (mg/mL)
0	30	0
33		15
50		30
60		45
67		60
75		90
80		120

60 cm^3/min, the exhaust flow rate to 550 cm^3/min and the atomiser flow rate to 600 cm^3/min, as optimised by Optomec Ltd..

The ink deposition was programmed by creating a shape on AutoCAD 2015 and then running the file using KEWA Motion 2.5.0 (Table 2). The KEWA VH Tools R2 plug in for AutoCAD was utilised to generate the appropriate circle fill for KEWA to follow, which took the form of a spiral starting from the outside of the circle and working inwards. The print speed was maintained at 3 mm/s. To build up layers and generate a 3D structure, the file was rerun until the desired height was reached. Printer capabilities were tested by programming different shapes and sizes via the KEWA Motion 2.5.0, and different nozzle sizes (150, 200, 250 and 300 μm). The print stage was maintained at ambient temperatures to avoid potential temperature induced phase transformation or additional polymer swelling. Ink was printed on to different substrates depending on the needs of the study. Rice paper was used for powder x-ray diffraction (PXRD) and Ultra High Performance Liquid Chromatography (UHPLC), and the ink was printed directly into 25 μl aluminium pans for differential scanning calorimetry (DSC), onto glass coverslips for contact angle, onto custom made sample cups for dissolution, and onto aluminium stubs for scanning electron microscopy (SEM). Care was taken to ensure substrates were completely free of dust or contamination to limit substrate effects on inkjet printed materials (Genina et al., 2013; Planchette et al., 2016). Process drift was minimised by ensuring the atomiser jet inlet was always a minimum of 1 mm below the surface of the ink within the pneumatic atomiser chamber. Should less ink ever be required borosilicate beads were added to the bottom of the chamber to reduce the atomiser volume. Future work could develop this through modification of the pneumatic atomiser chamber (Tafoya and Secor, 2020).

2.2.3. Optical microscopy

Images of the printed outputs were taken using a Leica DM6000M Automated Research Microscope coupled with the Leica Application Suite (Leica Microsystems Ltd., Milton Keynes, U.K.). A 2.5x objective was utilised with a differential interference contrast method utilising the transmitted light source for optimum representation of material distribution.

2.2.4. Ultra high pressure liquid chromatography

Ultra high pressure liquid chromatography (UHPLC) was carried out using an Agilent 1290 UHPLC, 6530 Q-TOF (Agilent Technologies, Santa Clara, California, USA) with detection at 280 nm and a mobile phase consisting of acetonitrile: water (pH 2.5 H_3PO_4) 80:20 running at 1 ml/min on a C-18(2) 100 Å silica reversed phase column. Samples were prepared by printing on rice paper for ease of dissolution and dissolved in 10 ml acetonitrile. Calibration curves covering a range of 5–100 μg/ml were produced for each UHPLC session using the area under the curve and concentrations of samples were calculated using the resultant equation of the line. The chromatographs were collected using MassHunter Workstation Software Data Collection and Qualitative Analysis B.07.00.

Table 2
Printer deposition design specifications.

Deposition diameter (mm)	Line length (mm, circumference and infill)	Area based on 250 μm diameter nozzle (mm^2)	Area based on 300 μm diameter nozzle (mm^2)	Use
2	32.54	8.14	9.76	Dissolution, scaling by area
5	199.78	49.94	59.93	Scaling, distribution, thickness, Raman, DSC, SEM
7	389.77	97.44	116.93	Scaling by area
10	792.53	198.13	237.76	Scaling by area, PXRD
20	3155.63	788.91	946.69	Contact angle

2.2.5. Depth analysis by laser triangulation

Printed samples were measured by laser triangulation using an LK-H057 (Keyence Corporation of America, Illinois, USA). Samples were analysed by initially taking a background measurement of the rice paper and then moving the sample so the centre was in line with the laser. Sample height was then collected on the LK-navigator software and compared.

2.2.6. Powder x-ray diffraction

Powder x-ray diffraction (PXRD) was carried out using a Bruker D8 Discover X-ray diffractometer (Bruker Corporation, Massachusetts, USA). Samples were printed onto rice paper and the signal generated by the rice paper was subtracted using the analysis software Diffrac. EVA. Samples were tested over a range of 5-35°2θ at 0.01 s. Samples were analysed using DIFFRAC.EVA.V4.1. Samples were stored for 6 months under ambient conditions and analysed again at 2 days, 5 days, 8 days, 15 days, 22 days, 29 days, 60 days and 180 days.

2.2.7. Differential Scanning calorimetry

Differential Scanning Calorimetry (DSC) was carried out using a Netzsch STA449 F1 Jupiter (NETZSCH-Gerätebau GmbH, Wolverhampton, West Midlands, UK). Powder samples were prepared in the standard manner, weighing the aluminium pans before and after loading. Dosage form samples were prepared by printing directly into the pans for a period of 20 min to produce samples of 1 – 5 mg. All samples were run in pierced pans. Analysis was carried out over a range of room temperature to 150℃, over 30 min, cooling with liquid nitrogen between samples. Results were analysed using Netzsch Analyser.

2.2.8. Scanning Electron microscopy

Scanning Electron Microscopy (SEM) was carried out using a U9320B Filed Emission Scanning Electron Microscope (Keysight, USA) using back scattering mode. Ink was deposited directly on to SEM stubs, using a 2 mm circular deposition pattern (Table 2), before the samples were subjected to a 20 nm gold coat and then measured at x1,500 magnification.

2.2.9. Contact angle

Samples were tested for wettability using a Krüss DSA 100 Drop Size Analyser (Krüss, Hamburg, Germany) by applying 20 μL droplets to the surface using a 0.7 mm needle. The instrument was driven and samples were analysed using the Krüss software Drop Size Analysis. A deionised water drop was initially created on the needle surface and then the needle was lowered until it was just above the sample surface, as observed in the drop window. A video recording was started and then the needle was lowered until the droplet detached onto the sample surface. The changes in the sample were observed in real time on the video and once recorded the video was analysed. The point of initial contact was established and this was designated point zero. The baseline was then lined up with point zero and the contact angle measured. Care was taken to ensure the measurement reflected the shape of the actual droplet. Due to the nature of the samples utilised in this study the results were based on the initial contact angle taken at point zero.

2.2.10. Dissolution Testing

Drug release and intrinsic dissolution rate were measured using a Sirius Surface Dissolution Imager I (SDI I) with a 280 nm UV filter (Sirius Analytical Instruments Ltd., Forrest Row, East Sussex, U.K.). Samples were tested in simulated intestinal fluid pH 6.8 (without enzymes) prepared following the standard British Pharmacopoeia methods

(British Pharmacopoeia Commission Secretariat of the Medicines and Healthcare Products Regulatory Agency, 2025). A molar extinction coefficient value was obtained by analysing 3 sets of standards over a range of 1 – 10 μg/ml prepared with dissolution buffer and 10 % (v/v) methanol. A similar method to a previously published study was utilised, manually infusing the flow cell with each standard in turn over a 20 min period (Etherson et al., 2020). Powder control compacts were prepared (using the standard Sirius Analytical method (Ward et al., 2017)), by adding the powders to the sample cup within the micro-compressor die and compressed to two clicks using the torque wrench at 60 cN.m for 10 min. Samples were then added to the SDI flow cell and media was passed over the surface of the sample cup for 20 min at 0.2 ml/min. Formulations were printed directly into sample cups (Paraytec Ltd., York, U.K.). Drug release was observed using the program Sirius Data Analyser, recording the absorbance over time. Samples were then analysed using this data analysis software with the average molar extinction coefficient and molecular mass values for fenofibrate (14831 M^{-1} cm^{-1} and 360.83 g/mol respectively).

2.2.11. Statistical analysis

Results were plotted and statistical analysis was carried out using Origin Pro 2017, values presented as mean ± standard error with the number of replicates as stated.

3. Results and Discussion

3.1. Ink and printing properties

3.1.1. Ink rheology

The ink formulations showed an increase in viscosity with polymer concentration as demonstrated by a comparison of the viscosity taken at the shear rate value of 1000 s^{-1} (Fig. 1). The relationship was linear with the exception of the latter two concentrations which demonstrated a rise to the curve in a more exponential fashion. Statistical analysis in Origin Pro 2017 gave a P-value of 5.95 × 10^{-5} suggesting the relationship between polymer concentration and viscosity was significant. This relationship between PVP viscosity and concentration has been observed a number of times in the literature such as in water comparing K-values (Mehrdad et al., 2013; Swei and Talbot, 2002) and with cerium (III) 2,4-pentadionate hydrate and zirconium(IV) 2,4-pentadionate in propionic acid comparing high molecular weight and low molecular weight PVP (Calleja et al., 2014). Fenofibrate and PVP have also previously been studied for viscosity in the literature but only in a 50:50 ethanol and dichloromethane solution with 20 % w/w solute content (Ng et al., 2013). Therefore, although there is no direct comparison for the system under study, the behaviour was consistent with the literature and the inks within the required printer performance parameters.

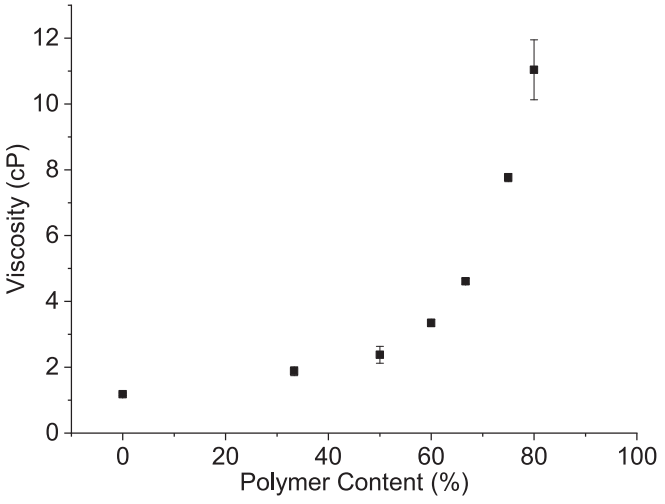

Fig. 1. The effect of PVP concentration on ink viscosity. Viscosity measured at 1000 s^{-1}, drug concentration 30 mg/ml, n = 3 ± standard error.

3.1.2. Optical microscopy

An example printed dosage form can be observed in Fig. 2. The spiral printer pattern governed by KEWA were clearly seen, as were the particles which formed the overall structure. There was some suggestion of the coffee ring effect associated with inkjet printing which has been seen previously in the literature both in aerosol jet (Seifert et al., 2015; Tait et al., 2015) and more traditional inkjet printing (Jabari and Toyserkani, 2015; Luan et al., 2016). However, the spiral pattern did ensure the material was distributed throughout the dosage form in a consistent manner.

3.1.3. Drug content control

Fig. 3 demonstrates the various measures by which drug content can be controlled using the aerosol jet technique. Nozzle size showed a linear relationship with mass of drug deposited with an r-squared value of 0.92. On statistical analysis a P-value of 0.04 was obtained confirming there was a significant relationship between nozzle size and drug mass deposited. Changing the nozzle size from the minimum to the maximum allowed a 3-fold increase in mass deposited, with the error slightly higher for the smaller nozzle sizes. Significant differences were recorded on performing an ANOVA where the 150 to 200 μm nozzles showed a P-value of 2.29 × 10^{-3} Nozzle size was very dependent on the manufacturer's stated nozzle diameters and, as it was such a small scale, any slight variation was magnified. Thus, there was a chance of variation between nozzles of the same size and a chance that nozzles were not exactly the size specified. Nozzles of 150 and 200 μm also suffered from bigger variations between samples as they were less forgiving of viscosity and thus droplet size than 250 and 300 μm as exhibited by bigger error bars than the latter two nozzle sizes. Although there is little evidence of study of the relationship between nozzle size and mass previously, nozzle size has been studied as a means of changing droplet size in piezoelectric printers (Liou et al., 2010). Linearity was observed between the droplet size and nozzle size which may explain the linearity between nozzle size and mass observed in the current study. The effect of nozzle size on deposition has been previously demonstrated in another aerosol jet system, the Optomec Aerosol Jet M^3D Printer, with 100, 150 and 200 μm nozzles. However, this was with silver ink and thus, although changes in the line width were observed, it was not directly

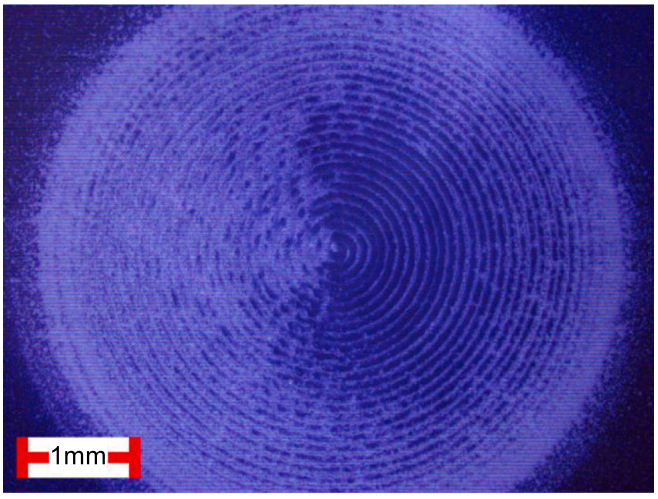

Fig. 2. Image of printed fenofibrate and PVP K30 with 75 % (w/w solute) polymer. Captured using a Leica DM6000M Automated Research Microscope at 2.5x objective, with a differential interference contrast method and a transmitted light source.

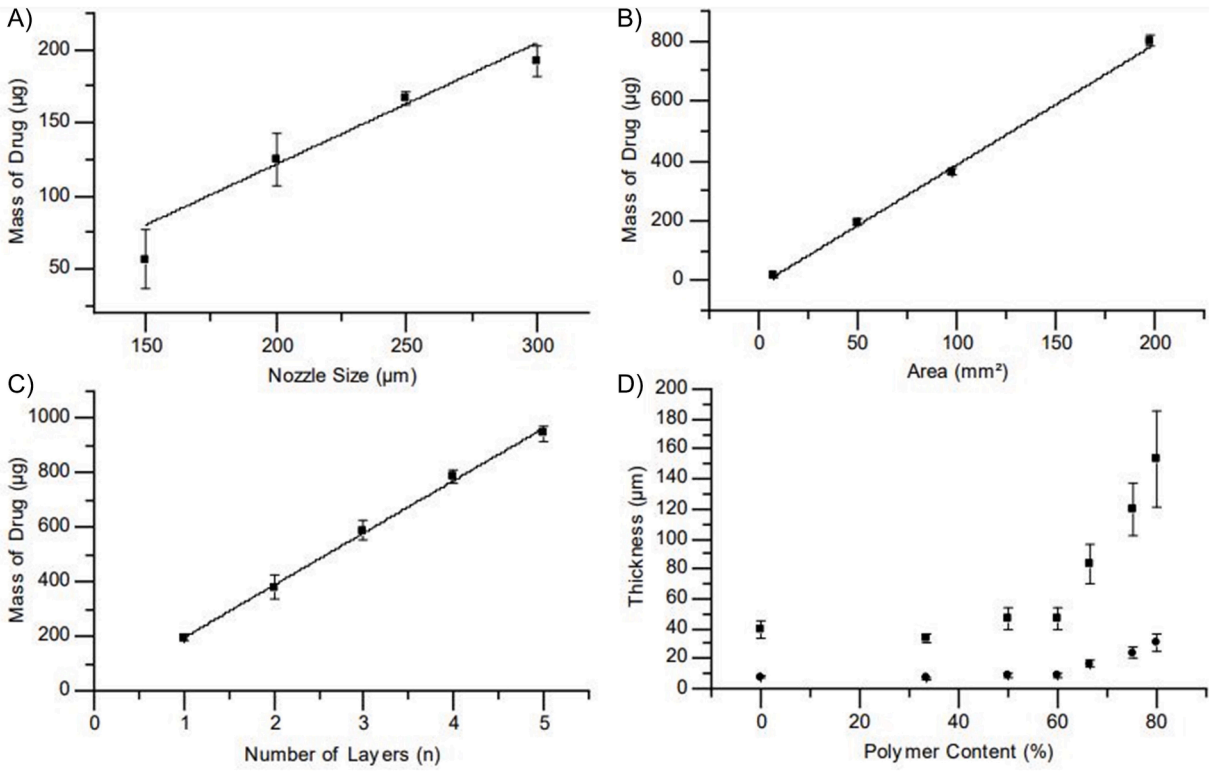

Fig. 3. Printed Drug Content Control. A): Effect of nozzle size on printed drug mass, printed with nozzle sizes 150, 200, 250 and 300 µm at 3 mm/s to print a 5 mm diameter circle, $r^2 = 0.91999$. B): Effect of deposition area on printed drug mass, printed with a 250 µm nozzle at 3 mm/s to print a 5 mm diameter circle, $r^2 = 0.99869$. N.B. Some error bars are located within the points. C): Effect of layer number on printed drug mass, printed with a 250 µm nozzle at 3 mm/s to print 5 mm diameter circles, $r^2 = 0.99903$. D): Deposition thickness, based on polymer content as detected by laser triangulation of five layers (triangle) and theoretical one layer (circle) samples, n = 3 ± standard error. In all cases ink contained fenofibrate:PVP K30 with 50 % (w/w solute) polymer, n = 6 ± standard error, unless otherwise stated.

comparable with API mass (Mahajan et al., 2013).

Deposition area was found to be linear and highly reproducible as the error bars are often too small to be observed (Fig. 3), which may be due to the fact that deposition area can be designed with micrometre resolution in AutoCAD. On statistical analysis a P-value of 6.58×10^{-4} was obtained suggesting a significant relationship between area and mass of drug deposited. On increasing the area deposited, up to a 40-fold increase in the drug mass deposited was achieved. On performing an ANOVA all the samples showed a P-value of 0.00 suggesting changing the size has significant effects. This demonstrates potential for generating personalised dosing. Changing the area of deposition to alter the dose has been employed previously in a personalised medicine context by thermal inkjet printing warfarin using a Hewlett-Packard (HP) 5940 Deskjet. Printing 0.5 × 1-7 cm was shown to result in a fully linear relationship between the length and drug mass (Vuddanda et al., 2018).

Layering depositions to generate dosage forms resulted in linearity (Fig. 3) with the average deposited drug mass approximately 200 µg per layer and statistical analysis (P-value of 1.29×10^{-5}) confirming a significant relationship between the layer number and mass deposited. This result arose since applying the same AutoCAD drawing for each layer eliminated program dependent issues and using the same nozzle size eliminated any manufacturer dependent variation. Unlike other ink jet printers (Wickström et al., 2015), material was not lost by using this method as the dragging action was eliminated by the free moving stage. Thus, layering in this manner demonstrates potential for generating personalised dosing. Generally, previous printing papers have reported layering but have often failed to demonstrate linearity (Akagi et al., 2014; Wickström et al., 2015). One exception to this was a paper by Vakili et al. (2015) which showed a linear relationship between the number of layers of theophylline and glycerine printed by thermal inkjet printing and the resultant drug loading detected, enabling effective personalised medicine (Vakili et al., 2015). Layering has also been demonstrated using an aerosol jet printer previously with silver ink (Kopola et al., 2012) and with barium titanate based multilayer ceramic capacitors (Folgar et al., 2011) but never with active pharmaceutical ingredients and thus this finding was novel.

Laser triangulation allows measurement of deposition thickness (Fig. 3). It was not possible to measure and separate a single layer thickness from the substrate thickness, therefore five layer samples were utilised and a calculated single layer was presented for comparison. The thickness of the deposition mimicked the exponential curve of the rheology trend seen in Fig. 1 in that there was an initial gentle slope up to 60 % (w/w) polymer before a rapid increase. Samples of increasing polymer content demonstrated similar exponential relationships with both rheology and thickness. These properties have been linked in a previous paper looking into the relationship between deposition thickness and rheology of PVP by Calleja et al. A semi-log plot illustrated an exponential increase in viscosity with concentration of PVP solutions and similar plot of concentration against thickness was observed on spin coating (Calleja et al., 2014).

It should be noted that variations between samples in terms of detected drug content and thickness of samples could also be attributed to the principle of system drift, despite minimisation. This is a phenomenon observed in aerosol jet printing where the deposition varies over time (Tafoya and Secor, 2020; Yoo et al., 2021). It is believed to be due to variations in flow and the supply of ink within the atomiser. This has been observed in a number of papers previously, however largely only using the ultrasonic atomiser (Hines et al., 2021; Tafoya and Secor, 2020; Yoo et al., 2021). This could potentially be overcome by addition of a circulating ink system, however future work into minimising line blockages would be required (Dai and Zhejiang Flashforge Group Co. Ltd., 2023; de Danda et al. (2019), Fu and Wuxi Light Industry Univ

Printing Factory, 2020; Sui et al., 2023; Xu et al., 2023).

3.2. Solid state properties

PXRD showed significant effects of printing the drug and polymer together. Fig. 4 compares drug, and drug/polymer physical mixtures, where the crystalline drug related peaks were observed to reduce with polymer content but did not fully disappear. For the printed drug and drug/polymer mixtures, increasing polymer content reduced the crystallinity of the overall formulation gradually until a fully amorphous product was achieved on printing formulations with a 75 % (w/w) polymer content or higher system F & G in Fig. 4. Furthermore, Table 3 demonstrates that this loss of crystallinity was retained for 6 months and thus these solid dispersions can be considered stable. DSC showed a loss in crystallinity in the physical mixtures with polymer content but it was more a reflection of the mass of drug present rather than the formation of amorphous material (Fig. 4). The printed samples showed a gradual loss of the crystalline peak as amorphous material was formed with higher polymer content, with the signal disappearing in system E where the PXRD still detected crystalline drug.

As can be observed in the SEM images (Fig. 5), the formulations with lower concentrations of PVP continued to exhibit a degree of crystallinity, with the addition of 33 % (w/w solute) polymer resulting in a change from 'driftwood' like crystalline particles to more plate-like and elongated crystals. On addition of 50 % (w/w solute) polymer the drug started to form cuboidal and squamous crystals with a light covering of polymer. On addition of 60 % (w/w solute) polymer the drug started to agglomerate more with large crystalline particles and amorphous

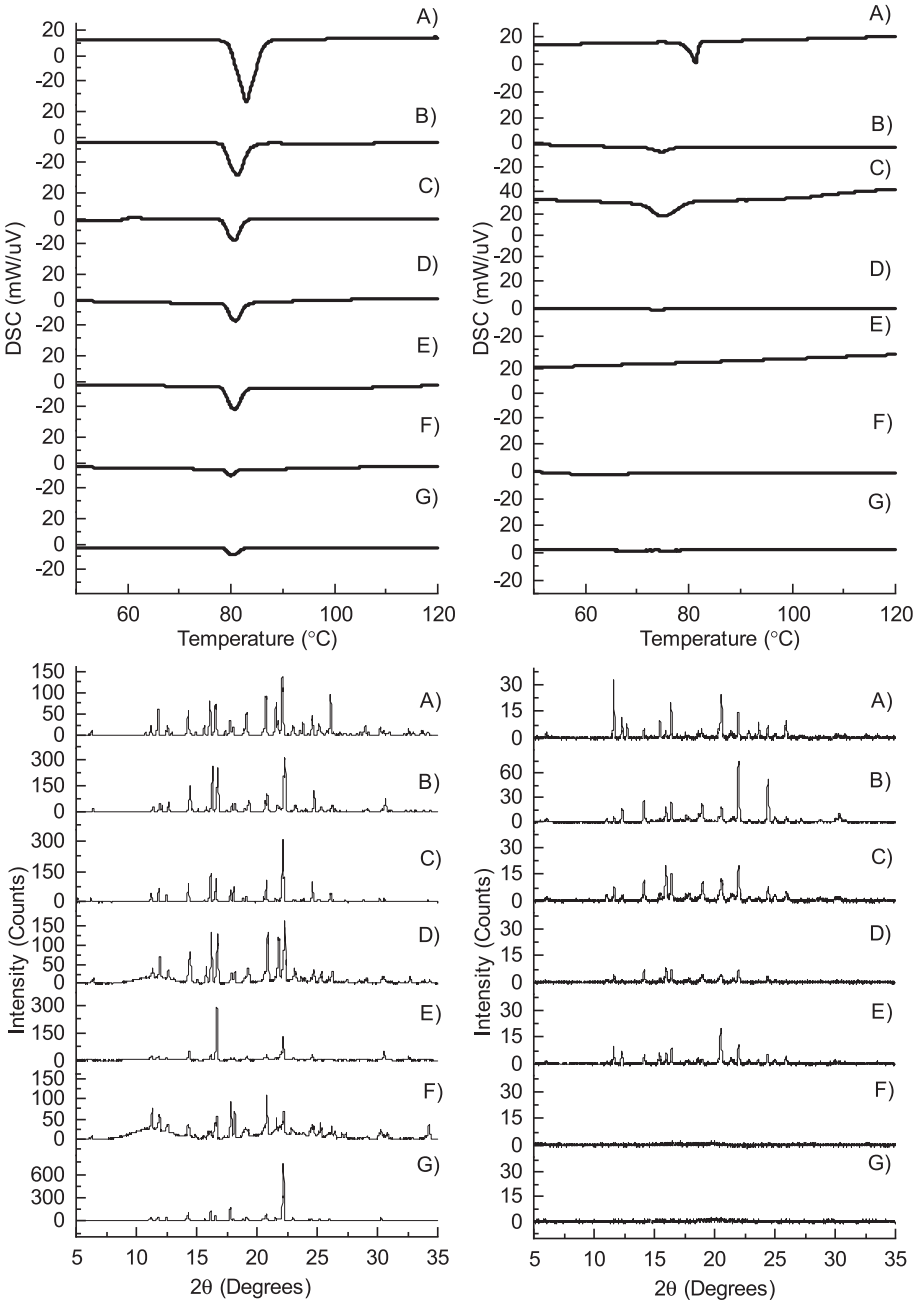

Fig. 4. Solid State Analysis of Printed Output. Powdered samples (left) and printed samples (right). Top panels: DSC of (A) fenofibrate and mixtures of fenofibrate and PVP K30 with (B) 33% (C) 50%, (D) 60%, (E) 67%, (F) 75% and (G) 80% (w/w solute) polymer content, Bottom panels.X-ray diffraction patterns of (A) fenofibrate and mixtures of fenofibrate and PVP K30 with (B) 33% (C) 50%, (D) 60%, (E) 67%, (F) 75% and (G) 80% (w/w solute) polymer content.

Table 3
PXRD Peak Count of printed samples over 6 months, where n = 1.

Polymer Content (%, w/w solute, where API = 30 mg/ml)	Peak Count (n)								
	Day 1	Day 2	Day 5	Day 8	Day 15	Day 22	Day 29	Day 60	Day 180
0	36	36	38	38	40	40	40	40	38
33	32	32	32	32	34	34	34	28	28
50	8	10	18	20	21	22	22	19	24
60	2	5	5	0	2	0	1	2	12
67	3	5	10	9	14	15	18	15	15
75	0	0	0	0	0	0	0	0	0
80	0	0	0	0	0	0	0	0	0

particles being observed. However, on increasing the polymer concentration to 67 % (w/w solute) the formulation started to appear more amorphous with only slight crystallinity present (< 5 % visual assessment). Ultimately on addition of 75 % and 80 % (w/w solute) polymer the formulation was fully amorphous as characterised by spherical particles throughout (Xia et al., 2016), and in agreement with the PXRD and DSC results discussed above.

Previous studies have demonstrated similar solid state changes on spray drying fenofibrate with polymers. Vogt et al. investigated nanosizing in conjunction with spray drying of fenofibrate, leading to complete loss of crystallinity on analysis by x-ray diffraction (Vogt et al., 2008). Varshosaz and Ghassami produced amorphous material on spray drying fenofibrate with Eudragit E100, Solutol HS15 and HPMC, analysed by x-ray diffraction and SEM (Varshosaz and Ghassami, 2015). Furthermore, Yousaf et al. supported the effect of printing in the absence of sufficient PVP with a similar effect on spray drying, where fully amorphous products failed to form as only 1:1.8 fenofibrate:PVP was present in the starting material (Yousaf et al., 2015). There is also previous evidence of the thermal effects of producing amorphous fenofibrate with PVP as demonstrated by Choi et al. using solvent evaporation with 1:1 fenofibrate and PVP (Choi et al., 2013).

The particle size formed on printing was largely governed by the viscosity of the starting ink. This study has shown the viscosity increased with polymer content and thus it should follow that the droplet size achieved on atomisation would also increase, increasing the overall particle size achieved. 75 % polymer (w/w solute) printed fenofibrate and PVP K30 samples exhibited larger particles than 50 % polymer (w/w solute) printed samples. 67 %, 75 % and 80 % polymer (w/w solute) printed samples exhibited larger agglomerates. This effect of viscosity on particle size has been observed previously in spray drying, which is highly significant as the aerosol jet is effectively a miniaturised version (Law et al., 2017; Sander and Penović, 2014). In terms of comparison of the solid state effects to inkjet printing in the literature, the closest comparison is a paper by Scoutaris et al. involving piezoelectric inkjet printing of felodipine and PVP in an ethanol:DMSO 95:5 solution, resulting in amorphous material as demonstrated by TOF-SIMS. However, unlike the current study, the amorphous state in Scoutaris et al. was found to be lost over the course of an extended spray time (Scoutaris et al., 2011). The effect of viscosity on particle size has also been previously observed on inkjet printing of mannitol, mannitol-ammonium bicarbonate mixtures and mannitol-ammonium bicarbonate-PTFE mixtures, where the overall spherical particle size increased with viscosity in an exponential fashion (Winter et al., 2023). However, there is no prior evidence of aerosol jet printing resulting in this effect. Thus it is extremely of note that this is the first study using aerosol jet printing to produce amorphous pharmaceutical material.

3.3. Contact angle

The effect of printing on wettability can be observed in Fig. 6. Printing fenofibrate in ethanol alone resulted in a high contact angle and poor wettability, which was to be expected as fenofibrate is virtually insoluble in water. The wettability increased considerably on addition of polymer with the addition of 33 % (w/w solute) polymer content causing the contact angle to fall from an average of 110.7° to 65.02°. This was supported by an ANOVA as the difference between this point and that of the fenofibrate has a P-value of 5.62×10^{-7}. The contact angle fell with increasing polymer content until 60 % (w/w solute) polymer content at an average of 43.24°, after which the graph was observed to level off with values of 45.67°, 30.52° and 40.87° for the 67 %, 75 %and 80 % (w/w solute) polymer content fenofibrate and PVP K30 samples respectively. This may be attributed to formation of amorphous particles of drug which were encased in the polymer increasing the overall wettability of the drug. Thus, the wettability may be considered solely a function of the polymer until 60 % (w/w solute) polymer content is present, where the amorphous particles began to play a part with the fully amorphous 75 % and 80 % (w/w solute) polymer content fenofibrate and PVP K30 samples, ultimately showing the greatest wettability overall.

3.4. Dissolution

Drug release achieved from control powder-based compacts of fenofibrate and PVP K30 (Fig. 7) resulted in an increase in drug release relative to drug alone with increasing polymer content. Ultimately, on addition of 80 % (w/w) polymer the release increased by 10-fold relative to the drug alone but the overall release was low, not reproducible between the compacts and did not increase in a linear fashion. For example, on addition of 33.3 % (w/w) polymer the release was lower than that of the drug alone, and samples with 60 % (w/w) polymer content exhibited a higher average release than those with 66.7 % (w/w) polymer content. On conducting an ANOVA, most of the samples did not exhibit a significant change from fenofibrate alone, with the exception of those containing 80 % (w/w) polymer content which had a P-value of 0.04.

The printed materials (Fig. 7), however, showed a 10- to 30-fold higher drug release relative to the comparable powder samples. The greatest release was achieved by the samples exhibiting amorphous particles, with the 60 % (w/w solute) polymer content fenofibrate and PVP K30 printed samples showing a substantial increase relative to the 50 % (w/w solute) polymer content samples, on initial amorphous particle formation. Furthermore, the 75 % (w/w solute) polymer content samples showed a statistically significant increase ($P = 4.0 \times 10^{-3}$) relative to the 67 % (w/w solute) polymer content samples on the complete loss of crystallinity. Ultimately, the 80 % (w/w solute) polymer samples showed the greatest increase overall with up to 4.3 % drug released in 20 min, a 40-fold increase relative to printed drug alone. The printed materials were also generally more reproducible than the powder compacts as demonstrated by smaller error bars overall.

In a similar manner to drug release, intrinsic dissolution rate increased with polymer content in the control compacts but the increase was no more than 5 μg/min/cm^2, however with printed material this increase was up to 40 μg/min/cm^2 (Fig. 8), showing nearly a 10-fold increase. The 67 %, 75 % and 80 % (w/w solute) polymer content samples showed the most notable difference as shown by an exponential increase in Fig. 8. This was supported by an ANOVA where 67 % (w/w

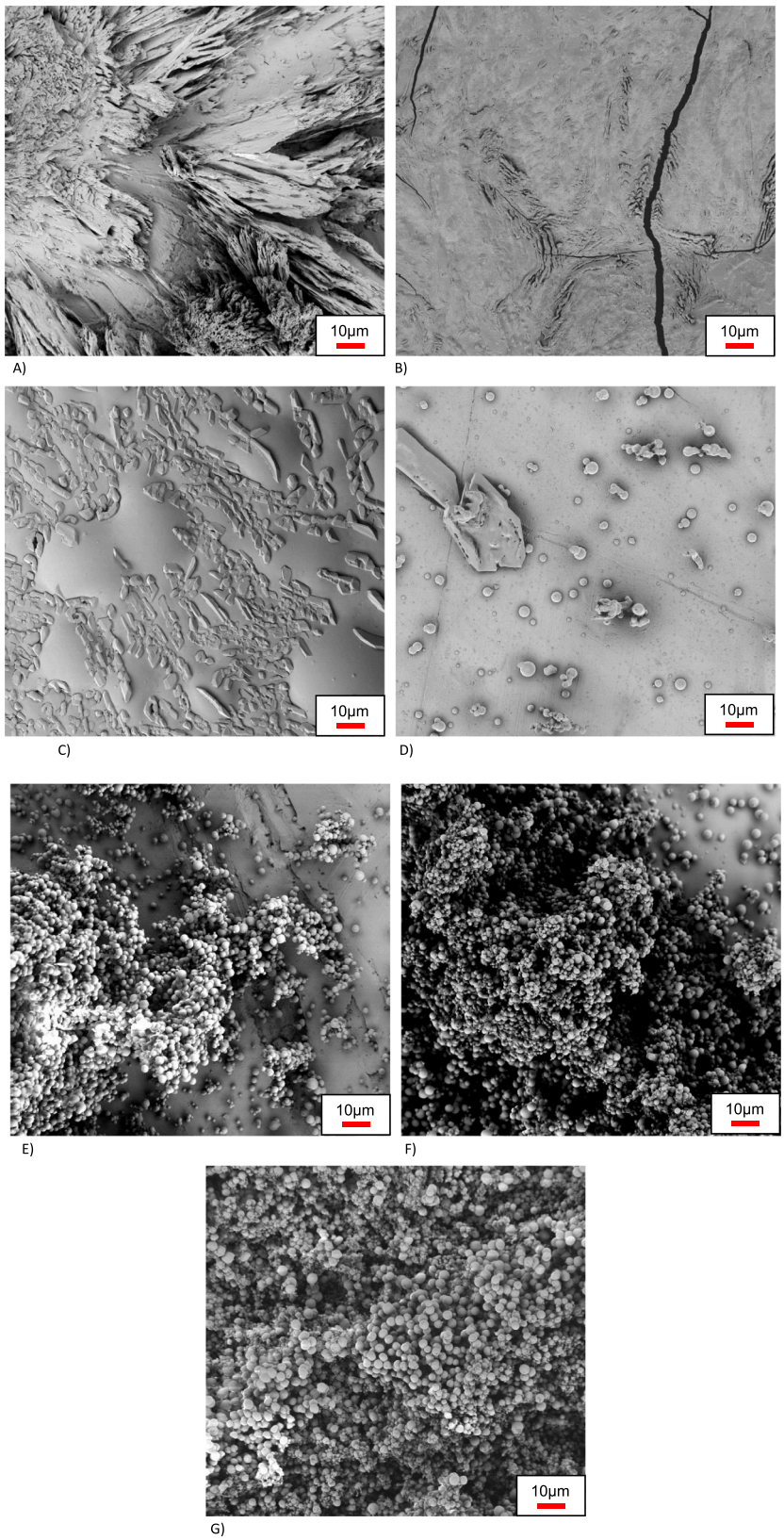

Fig. 5. Scanning Electron Micrographs of Printed Output. SEM of (A) fenofibrate and mixtures of fenofibrate and PVP K30 with (B) 33 % (C) 50 %, (D) 60 %, (E) 67 %, (F) 75 % and (G) 80 % (w/w solute) polymer. contenttaken at 1.5 K magnification with the size bar in blue showing 10 μm.

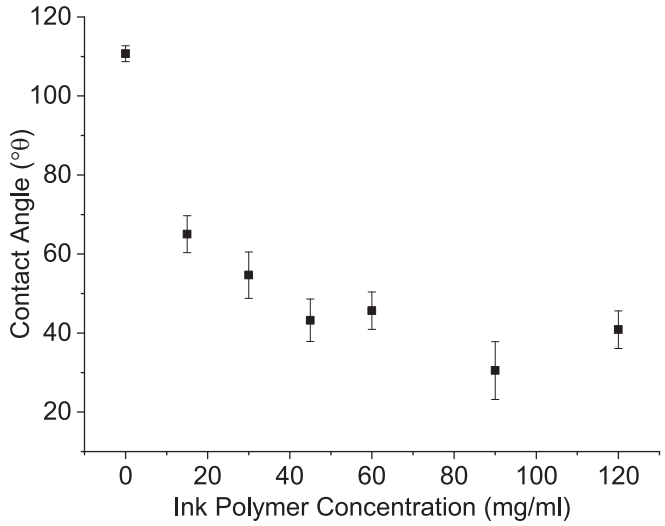

Fig. 6. Average contact angle values taken at point zero against polymer concentration of the starting ink where n = 9 ± standard error.

solute) polymer content samples were shown to have a P-value of 1.65 × 10^{-4}, 75 % (w/w solute) polymer content samples were shown to have a P-value of 2.72 × 10^{-6} and 80 % (w/w solute) polymer content samples were shown to have a P-value of 2.10 × 10^{-7} compared to their powder counter parts.

Overall, the formation of amorphous material had a significant effect on dissolution properties resulting in a 10- to 30-fold increase in dissolution relative to the comparable physical mixtures. Spray drying has demonstrated similar dissolution from fenofibrate and PVP based systems in previous studies. For example, Hugo et al. demonstrated a 10-fold increase in dissolution on spray drying fenofibrate with PVP K25 in a 1:3 ratio in ethanol, while Choi et al. demonstrated a 4-fold increase in dissolution on spray drying fenofibrate and PVP in a 1:1 ratio to form nanoparticles (Choi et al., 2013; Hugo et al., 2013). Increases in drug release from inkjet printed samples generated from fenofibrate in ethanol inks (Hossen et al., 2014; Vialpando et al., 2012) have been observed previously but interestingly inkjet printing the combination of fenofibrate and PVP in ethanol is not presented in the literature.

3.5. Aerosol ink jet printing – pharmaceutical application opportunities

The aerosol inkjet technology presented in this study successfully created amorphous, pharmaceutical dose forms with improved dissolution performance. The technology allows for flexible dosing, and would allow accurate dosing for high potency drugs: doses of 20 μg to 1 mg or greater as films (printing highly diluted solutions onto a substrate such as rice paper) and theoretically up to full size tablets (with tablet core weight ranging from 200–300 mg). High dose products with tablet core weights > 300 mg are very likely not viable, however, as the current process is too slow. Whilst Additive Manufacturing offers superior spatial resolution, it is a slow manufacturing process and cannot be compared to traditional pharmaceutical manufacturing processes, such as tablet production via a rotary tablet press. The current technology used in this study, would require further development to improve throughput for commercial manufacture. However, the scale and flexibility of this technology are advantageous for niche applications with either small patient populations or where personalisation is required, such as dose adjustments due to narrow therapeutic index of APIs or patient specific renal clearances (Boehm et al., 2014; Carou-Senra et al., 2023; Cheow et al., 2015; Kallakunta et al., 2020; Rodríguez-Pombo et al., 2024; Vuddanda et al., 2018). In addition, this technology would be advantageous for early phase clinical trials covering dose escalation studies. The model drug fenofibrate, is commercially available as a range of different oral solid dose forms (capsules, tablets and delayed release capsules) in a wide range of doses (e.g. a capsule formulation at nine different doses, ranging from 30 to 200 mg (Sidhu and Tripp, 2025) (Table 4). With dose adjustments for fenofibrate therapy being made at 4 to 8 week intervals, as well as the vast range of therapeutic doses commercially in use (which are not bio-equivalent), a flexible manufacturing approach such as an on-demand additive manufacturing process would be highly advantageous.

4. Conclusions

The printer technology used in the current study has never previously been applied in pharmaceutical manufacture and demonstrated a number of highly significant advantages over the existing inkjet technology. It enabled production of fully scalable dosage forms for potential use in a personalised medicine context. Printing resulted in the formation of a crystalline product on printing drug alone but on application of polymer this crystallinity was reduced and a fully amorphous solid dispersion was achieved on printing 75 % (w/w) polymer to 25 % (w/w)

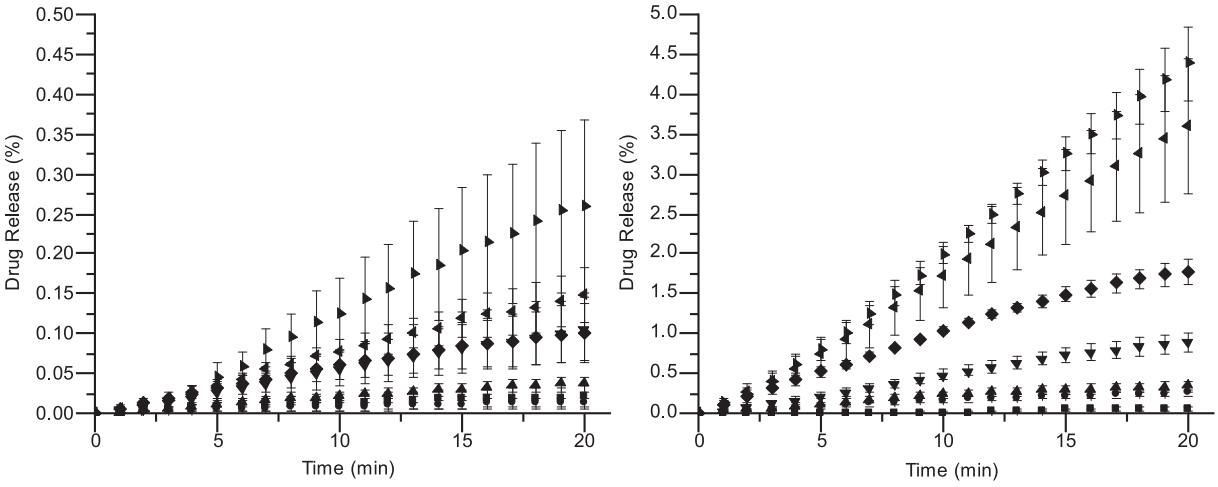

Fig. 7. Drug Dissolution from Powder Compacts and Printed Output. Percentage Drug Release from compacts (left) and printed samples (right) of fenofibrate (square) and, fenofibrate and PVP K30 with 33% (circle), 50% (up arrow), 60% (down arrow), 67% (rhombus), 75% (left arrow) and 80% (right arrow) (w/w solute) polymer content, n=3 ± standard error. The 67%, 75% and 80% (w/w solute) polymer content fenofibrate and PVP K30 printed systems are statistically significantly different to the powder compacts with P-values of 9.86x10^{-3}, 2.09x10^{-7} and 1.04x10^{-7} respectively.

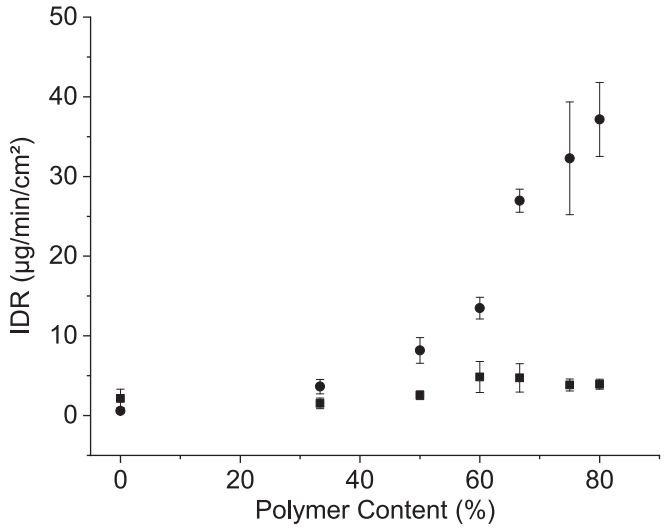

Fig. 8. Powder compacts (triangles) and printed materials (circles) against percentage polymer content, where n = 3 ± standard error. The 60 %, 67 %, 75 % and 80 %(w/w solute) polymer content fenofibrate and PVP K30 printed systems are statistically significantly different the powder compacts P-values of 3.33×10^{-3}, 1.05×10^{-5}, 4.07×10^{-7}, 1.17×10^{-7} respectively.

Table 4
Commercially available fenofibrate products and doses.

Dose Form	Doses available (mg)
Capsule of fenofibrate	30, 43, 50, 67, 90, 130, 134, 150, 200
Delayed-Release capsule of choline fenofibrate	45, 135
Tablet of feno-fibric acid	35, 105
Tablet of fenofibrate	40, 48, 54, 120, 145, 160

drug as shown by a number of solid state techniques. This allowed significantly increased dissolution of a poorly soluble compound as demonstrated by a 10- to 30-fold increase in drug release and intrinsic dissolution rate relative to comparable physical mixtures. These results demonstrated that aerosol jet printing as a unique system, was suitable for pharmaceutical applications and capable of high resolution printing with potential advantages over conventional ink jet printing for multi-layer systems. This may allow production of dosage forms for use in clinical trials, niche personalised dosing and other small scale applications. Despite limitations such as process drift, the careful choice of drug and polymer provided control of the drug's solid form properties in a manner equivalent to spray drying. This may hold potential in increasing the dissolution capabilities of a range of Class II drugs and thus could ultimately allow more drugs to progress through clinical trials. In addition, the 3D control and resolution provided by the instrument opened the potential for further applications such as the printing or coating of preformed structures, for example small medical devices. Aerosol jet printing is therefore worthy of further investigation for the production of pharmaceutical systems.

CRediT authorship contribution statement

Alice J. Turner: Writing – original draft, Methodology, Investigation, Formal analysis, Data curation. **Elke Prasad:** Writing – review & editing. **Alastair J. Florence:** Supervision. **Gavin W. Halbert:** Writing – review & editing, Supervision.

Declaration of competing interest

The authors declare that they have no known competing financial interests or personal relationships that could have appeared to influence the work reported in this paper.

Acknowledgements

The authors would like to acknowledge that unless otherwise stated this work was carried out in the CMAC National Facility, Glasgow supported by UKRPIF (UK Research Partnership Fund) award from the Higher Education Funding Council for England (HEFCE) (Grant ref HH13054), with the support of Deborah Bowering, Laura Harvey, Alan Martin and Monika Warzecha. The laser triangulation studies were carried out within The Centre for Structured Organic Particulate Systems (C-SOPS), Rutgers University, Piscataway, N.J. supported by the International Institute for Advanced Pharmaceutical Manufacturing (I2APM) (Grant ref EP/M02166/1), under the direction of Sonia Razavi. The liquid rheology and contact angle studies were carried out within AstraZeneca, Macclesfield under the supervision of Liz Meehan, Matt Bunker and Kevin Treacher. The authors would also like to thank the International Institute for Advanced Pharmaceutical Manufacturing (I2APM) (Grant ref EP/M02166/1) and the EPSRC Doctoral Training Centre in Continuous Manufacturing and Crystallisation (Grant ref EP/K503289/1) for funding this work. Gavin Halbert is funded by Cancer Research UK (C149/A20740).

References

Abt, M., Roch, A., Qayyum, J.A., Pestotnik, S., Stepien, L., Abu-Ageel, A., Wright, B., Ulusoy, A.C., Albrecht, J., Harle, L., Papapolymerou, J., Schuelke, T., 2018. Aerosol printed highly conductive Ag transmission lines for flexible electronic devices. IEEE Trans. Compon. Packaging. Manuf. Technol 8, 1838–1844. https://doi.org/10.1109/TCPMT.2018.2869977.

Akagi, T., Fujiwara, T., Akashi, M., 2014. Inkjet printing of layer-by-layer assembled poly (lactide) stereocomplex with encapsulated proteins. Langmuir 30, 1669–1676. https://doi.org/10.1021/la404162h.

Ako, H., O'Mahony, J., Hughes, H., McLoughlin, P., O'Reilly, N.J., 2023. A novel approach to the manufacture of dissolving microneedles arrays using aerosol jet printing. Appl. Mater. Today 35. https://doi.org/10.1016/j.apmt.2023.101958.

Ali, M.A., Hu, C., Zhang, F., Jahan, S., Yuan, B., Saleh, M.S., Gao, S.J., Panat, R., 2022. N protein-based ultrasensitive SARS-CoV-2 antibody detection in seconds via 3D nanoprinted, microarchitected array electrodes. J. Med. Virol 94, 2067–2078. https://doi.org/10.1002/jmv.27591.

Aoki, C., Ma, X., Higashi, K., Ishizuka, Y., Ueda, K., Kadota, K., Fukuzawa, K., Tozuka, Y., Kawakami, K., Yonemochi, E., Moribe, K., 2021. Stabilization mechanism of amorphous carbamazepine by transglycosylated rutin, a non-polymeric amorphous additive with a high glass transition temperature. Int. J. Pharm 600. https://doi.org/10.1016/j.ijpharm.2021.120491.

Arsenov, P.V., Efimov, A.A., Ivanov, V.V., 2021. Optimizing aerosol jet printing process of platinum ink for high-resolution conductive microstructures on ceramic and polymer substrates. Polymers. (basel) 13. https://doi.org/10.3390/polym13060918.

Bappy, M.O., Jiang, Q., Atampugre, S., Zhang, Y., 2024a. Aerosol jet printing of high-temperature multimodal sensors for strain and temperature sensing. ACS Appl. Nano. Mater 7, 9453–9459.

Bappy, M.O., Jiang, Q., Atampugre, S., Zhang, Y., 2024b. Aerosol jet printing of high-temperature bimodal sensors for simultaneous strain and temperature sensing using gold and indium tin oxide nanoparticle inks. ACS Appl. Nano. Mater 7, 9453–9459. https://doi.org/10.1021/acsanm.4c00907.

Boehm, R.D., Miller, P.R., Daniels, J., Stafslien, S., Narayan, R.J., 2014. Inkjet printing for pharmaceutical applications. Mater. Today 17, 247–252. https://doi.org/10.1016/j.mattod.2014.04.027.

British Pharmacopoeia Commission Secretariat of the Medicines and Healthcare Products Regulatory Agency, 2025. Appendix XII Recommendations on Dissolution Testing [WWW Document]. British Pharmacopoeia 2025 (Ph. Eur. 11.6 update). URL https://www-pharmacopoeia-com.proxy.lib.strath.ac.uk/bp-2025/appendices/appendix-12/appendix-xii-b–annex–recommendations-on-dissolution-testing.html?date=2025-01-01&text=dissolution (accessed 10.3.24).

Buanz, A.B.M., Saunders, M.H., Basit, A.W., Gaisford, S., 2011. Preparation of personalized-dose salbutamol sulphate oral films with thermal ink-jet printing. Pharm. Res 28, 2386–2392. https://doi.org/10.1007/s11095-011-0450-5.

Calleja, A., Ricart, S., Aklalouch, M., Mestres, N., Puig, T., Obradors, X., 2014. Thickness-concentration-viscosity relationships in spin-coated metalorganic ceria films containing polyvinylpyrrolidone. J. Solgel. Sci. Technol 72, 21–29. https://doi.org/10.1007/s10971-014-3417-2.

Carou-Senra, P., Ong, J.J., Castro, B.M., Seoane-Viaño, I., Rodríguez-Pombo, L., Cabalar, P., Alvarez-Lorenzo, C., Basit, A.W., Pérez, G., Goyanes, A., 2023. Predicting pharmaceutical inkjet printing outcomes using machine learning. Int. J. Pharm. X 5. https://doi.org/10.1016/j.ijpx.2023.100181.

Carou-Senra, P., Rodríguez-Pombo, L., Awad, A., Basit, A.W., Alvarez-Lorenzo, C., Goyanes, A., 2024. Inkjet Printing of Pharmaceuticals. Adv. Mater. https://doi.org/10.1002/adma.202309164.

Cheow, W.S., Kiew, T.Y., Hadinoto, K., 2015. Combining inkjet printing and amorphous nanonization to prepare personalized dosage forms of poorly-soluble drugs. Eur. J. Pharm. Biopharm. 96, 314–321. https://doi.org/10.1016/j.ejpb.2015.08.012.

Choi, J.H., Lee, K., Hong, S., Lee, S.K., Oh, Y.-K., Choi, S.K., Choi, H.-G., 2013. Effect of biocompatible polymers on the physicochemical and dissolution properties of fenofibrate in nanoparticle system. J. Pharm. Investig 43, 507–512. https://doi.org/10.1007/s40005-013-0100-5.

Davies, M., Hobbs, M.J., Nohl, J., Davies, B., Rodenburg, C., Willmott, J.R., 2024. Aerosol jet printed ionic liquid-doped polymer dispersed liquid crystal devices in optical systems, in: Khoo, I.C. (Ed.), Liquid Crystals XXVIII. SPIE, p. 57. doi: 10.1117/12.3032548.

Dai, Y., Zhejiang Flashforge Group Co. Ltd., 2023. Integrated 3D ink-jet printing circulating ink supply device. CN220180166U.

Daly, R., Harrington, T.S., Martin, G.D., Hutchings, I.M., 2015. Inkjet printing for pharmaceutics – A review of research and manufacturing. Int. J. Pharm. [epub. in. a. https://doi.org/10.1016/j.ijpharm.2015.03.017.

de Alencar Danda, L.J., de Medeiros, Batista L., Melo, V.C., Sobrinho, J.L., Soares, M.F., 2019. Combining amorphous solid dispersions for improved kinetic solubility of posaconazole simultaneously released from soluble PVP/VA64 and an insoluble ammonio methacrylate copolymer. Eur. J. Pharma. Sci. 133, 79–85. https://doi.org/10.1016/j.ejps.2019.03.012.

De Silva, M.N., Paulsen, J., Renn, M.J., Odde, D.J., 2006. Two-step cell patterning on planar and complex curved surfaces by precision spraying of polymers. Biotechnol. Bioeng 93, 919–927. https://doi.org/10.1002/bit.20787.

Deiner, L.J., Jenkins, T., Howell, T., Rottmayer, M., 2019. Aerosol Jet Printed Polymer Composite Electrolytes for Solid-State Li-Ion Batteries. Adv. Eng. Mater 21. https://doi.org/10.1002/adem.201900952.

Etherson, K., Dunn, C., Matthews, W., Pamelund, H., Sanderson, N., Izumi, T., Mathews, C., Halbert, G., Wilson, C., Mcallister, M., Mann, J., Butler, J., Khadra, I., 2020. An interlaboratory investigation of intrinsic dissolution rate determination using surface dissolution. Eur. J. Pharm. Biopharm. https://doi.org/10.1016/j.ejpb.2020.02.005.

Feng, J.Q., Ramm, A., Renn, M.J., 2021. A quantitative analysis of overspray in Aerosol Jet® printing. Flexible Printed Electron. 6. https://doi.org/10.1088/2058-8585/ac3019.

Folgar, C.E., Suchicital, C., Priya, S., 2011. Solution-based aerosol deposition process for synthesis of multilayer structures. Mater. Lett 65, 1302–1307. https://doi.org/10.1016/j.matlet.2011.01.069.

Fu, Q., Wuxi Light Industry Univ Printing Factory, 2020. Printing ink circulating treatment ink box. CN212242621 (U).

Gamba, L., Lajoie, J.A., Sippel, T.R., Secor, E.B., 2023. Multi-Material Aerosol Jet Printing of Al/Cuo Nanothermites for Versatile Fabrication of Energetic Antennas. Adv. Funct. Mater 33. https://doi.org/10.1002/adfm.202304060.

Genina, N., Fors, D., Palo, M., Peltonen, J., Sandler, N., 2013. Behavior of printable formulations of loperamide and caffeine on different substrates—Effect of print density in inkjet printing. Int. J. Pharm 453, 488–497. https://doi.org/10.1016/j.ijpharm.2013.06.003.

Goh, G.L., Agarwala, S., Yeong, W.Y., 2018. High resolution aerosol jet printing of conductive ink for stretchable electronics. In: Proceedings of the International Conference on Progress in Additive Manufacturing. pro-AM, pp. 109–114. https://doi.org/10.25341/D4FS3W.

Goh, G.L., Dikshit, V., Koneru, R., Peh, Z.K., Lu, W., Goh, G.D., Yeong, W.Y., 2022. Fabrication of design-optimized multifunctional safety cage with conformal circuits for drone using hybrid 3D printing technology. Int. J. Adv. Manuf. Technol. 120, 2573–2586. https://doi.org/10.1007/s00170-022-08831-y.

Gramlich, G., Huber, R., Häslich, F., Bhutani, A., Lemmer, U., Zwick, T., 2023. Process considerations for Aerosol-Jet printing of ultra fine features. Flexible Printed. Electron. 8. https://doi.org/10.1088/2058-8585/ace3d8.

Hines, D.R., Gu, Y., Martin, A.A., Li, P., Fleischer, J., Clough-Paez, A., Stackhouse, G., Dasgupta, A., Das, S., 2021. Considerations of aerosol-jet printing for the fabrication of printed hybrid electronic circuits. Addit. Manuf 47. https://doi.org/10.1016/j.addma.2021.102325.

Hossen, S.M.M., Sarkar, R., Towhid, H.A., Sultan, T., Aziz, N.M.A., 2014. Study on the effect of different polymers on in-vitro dissolution profile of Fenofibrate by solid dispersion technique. J. Appl. Pharm. Sci 4, 56–60. https://doi.org/10.7324/JAPS.2014.40608.

Hugo, M., Kunath, K., Dressman, J., 2013. Selection of excipient, solvent and packaging to optimize the performance of spray-dried formulations: case example fenofibrate. Drug. Dev. Ind. Pharm 39, 402–412. https://doi.org/10.3109/03639045.2012.685176.

Hyun, W.J., Secor, E.B., Rojas, G.A., Hersam, M.C., Francis, L.F., Frisbie, C.D., 2015. All-printed, foldable organic thin-film transistors on glassine paper. Advanced. Materials 27, 7058–7064. https://doi.org/10.1002/adma.201503478.

Jabari, E., Toyserkani, E., 2015. Micro-scale aerosol-jet printing of graphene interconnects. Carbon. N. Y 91, 321–329. https://doi.org/10.1016/j.carbon.2015.04.094.

Kallakunta, V.R., Sarabu, S., Bandari, S., Batra, A., Bi, V., Durig, T., Repka, M.A., 2020. Stable amorphous solid dispersions of fenofibrate using hot melt extrusion technology: Effect of formulation and process parameters for a low glass transition temperature drug. J. Drug. Deliv. Sci. Technol 58. https://doi.org/10.1016/j.jddst.2019.101395.

Kawabata, Y., Wada, K., Nakatani, M., Yamada, S., Onoue, S., 2011. Formulation design for poorly water-soluble drugs based on biopharmaceutics classification system: basic approaches and practical applications. Int. J. Pharm 420, 1–10. https://doi.org/10.1016/j.ijpharm.2011.08.032.

Kopola, P., Zimmermann, B., Filipovic, A., Schleiermacher, H.F., Greulich, J., Rousu, S., Hast, J., Myllylä, R., Würfel, U., 2012. Aerosol jet printed grid for ITO-free inverted organic solar cells. Solar Energy Mater. Solar Cells 107, 252–258. https://doi.org/10.1016/j.solmat.2012.06.042.

Lan, X., Lu, X., Chen, M.Y., Scherrer, D., Chung, T., Nguyen, E., Lai, R., Tice, J., 2017. Direct on-chip 3-D aerosol jet printing with high reliability. IEEE Trans. Compon. Packaging. Manuf. Technol 7, 1369–1376. https://doi.org/10.1109/TCPMT.2017.2710957.

Law, J., Kong, K.W., Chan, H.Y., Sun, W., Li, W.J., Chau, E.B.F., Chan, G.K.M., 2017. Atomization of high-viscosity fluids for aromatherapy using micro-heaters for heterogeneous bubble nucleation. Sci. Rep 7, 1–14. https://doi.org/10.1038/srep40289.

Liou, T.-M., Chan, C.-Y., Shih, K.-C., 2010. Effects of actuating waveform , ink property , and nozzle size on piezoelectrically driven inkjet droplets. Microfluid. Nanofluidics 8, 575–586. https://doi.org/10.1007/s10404-009-0488-4.

Lopez-Hallman, R., Rodriguez, R., Lai, Y.T., Zhang, Q., Tsao, B.H., Deiner, J., Fellner, J. P., Zhu, Y., 2024. All-Solid-State Battery Fabricated by 3D Aerosol Jet Printing. Adv. Eng. Mater 26. https://doi.org/10.1002/adem.202300953.

Luan, E., Zheng, Z., Li, X., Gu, H., Liu, S., 2016. Inkjet-assisted layer-by-layer printing of quantum dot/enzyme microarrays for highly sensitive detection of organophosphorous pesticides. Anal. Chim. Acta 916, 77–83. https://doi.org/10.1016/j.aca.2016.02.019.

Mahajan, A., Frisbie, C.D., Francis, L.F., 2013. Optimization of aerosol jet printing for high-resolution, high-aspect ratio silver lines. ACS. Appl. Mater. Interfaces 5, 4856–4864. https://doi.org/10.1021/am400606y.

Mehrdad, A., Shekaari, H., Niknam, Z., 2013. Fluid Phase Equilibria Effect of ionic liquid on the intrinsic viscosity of polyvinyl pyrrolidone in aqueous solutions. Fluid. Phase. Equilib 353, 69–75. https://doi.org/10.1016/j.fluid.2013.06.003.

Monne, M.A., Howlader, C.Q., Mishra, B., Chen, M.Y., 2021. Synthesis of printable polyvinyl alcohol for aerosol jet and inkjet printing technology. Micromachines. (basel) 12, 1–16. https://doi.org/10.3390/mi12020220.

Niu, Y., Wang, Z., Li, Y., Huang, B., Ma, T., Jiang, X., Cheng, H., Zhang, K., Yi, C., 2024. Ultrathin MXene/Ag-Ag Nanocomposite Films for 3D-Conformal Electromagnetic Shielding via Aerosol Jet Printing. SSRN. https://doi.org/10.2139/ssrn.5042994.

Overmeyer, L., Hohnholz, A., Suttmann, O., Kaierle, S., 2019. Multi-material laser direct writing of aerosol jet layered polymers. CIRP Annals 68, 217–220. https://doi.org/10.1016/j.cirp.2019.04.115.

Pandhi, T., Kreit, E., Aga, R., Fujimoto, K., Sharbati, M.T., Khademi, S., Chang, A.N., Xiong, F., Koehne, J., Heckman, E.M., Estrada, D., 2018. Electrical transport and power dissipation in aerosol-jet-printed graphene interconnects. Sci. Rep 8, 1–11. https://doi.org/10.1038/s41598-018-29195-y.

Pavec, M., Navratil, J., Soukup, R., Hamacek, A., 2018. A Bowtie Antenna Prepared by Aerosol Jet and Embroidering Technology. Proc. Int. Spring Seminar Electron. Technol. 2018-May, 1–4. doi: 10.1109/ISSE.2018.8443699.

Perilli, S., Di Pietro, M., Mantini, E., Regazzetti, M., Kiper, P., Galliani, F., Panella, M., Mantini, D., 2024. Development of a wearable electromyographic sensor with aerosol jet printing technology. bioengineering 11. doi: 10.3390/bioengineering11121283.

Planchette, C., Pichler, H., Wimmer-Teubenbacher, M., Gruber, M., Gruber-Woelfler, H., Mohr, S., Tetyczka, C., Hsiao, W.K., Paudel, A., Roblegg, E., Khinast, J., 2016. Printing medicines as orodispersible dosage forms: Effect of substrate on the printed micro-structure. Int. J. Pharm 509, 518–527. https://doi.org/10.1016/j.ijpharm.2015.10.054.

Rodríguez-Pombo, L., Carou-Senra, P., Rodríguez-Martínez, E., Januskaite, P., Rial, C., Félix, P., Alvarez-Lorenzo, C., Basit, A.W., Goyanes, A., 2024. Customizable orodispersible films: Inkjet printing and data matrix encoding for personalized hydrocortisone dosing. Int. J. Pharm 655. https://doi.org/10.1016/j.ijpharm.2024.124005.

Sander, A., Penović, T., 2014. Droplet Size Distribution Obtained by Atomization with Two-Fluid Nozzles in a Spray Dryer 2073–2084. doi: 10.1002/ceat.201400185.

Scoutaris, N., Alexander, M.R., Gellert, P.R., Roberts, C.J., 2011. Inkjet printing as a novel medicine formulation technique. J. Controlled. Release 156, 179–185. https://doi.org/10.1016/j.jconrel.2011.07.033.

Seifert, T., Sowade, E., Roscher, F., Wiemer, M., Gessner, T., Baumann, R.R., 2015. Additive manufacturing technologies compared: morphology of deposits of silver ink using inkjet and aerosol jet printing. Ind. Eng. Chem. Res 54, 769–779. https://doi.org/10.1021/ie503636c.

Serbest, B., Kara, S.G., Alpay, R., Ataşer, T., Kınacı, B., Akın Sönmez, N., Özçelik, S., 2024. Aerosol jet printing of flexible transparent conductive silver nanowire electrodes: effects of printing cycles. J. Electron. Mater. https://doi.org/10.1007/s11664-024-11615-7.

Sidhu, G., Tripp, J., 2025. Fenofibrate [WWW Document]. StatPearls Publishing, Treasure Island (FL) https://www.ncbi.nlm.nih.gov/books/NBK559219/ (accessed 1.7.25.

Sui, J., Chen, Y., Guangdong Juhan Printing Display Tech Co. Ltd., 2023. Ink jet pipeline, circulating ink jet device and ink circulating and processing method. CN116409063A.

Swei, J., Talbot, J.B., 2002. Viscosity Correlation for Aqueous Polyvinylpyrrolidone (PVP) Solutions 0–1.

Taccola, S., Bakhshi, H., Sanchez Sifuentes, M., Lloyd, P., Tinsley, L.J., Macdonald, J., Bacchetti, A., Cespedes, O., Chandler, J.H., Valdastri, P., Meyer, W., Harris, R.A., 2024. Dual-Material Aerosol Jet Printing of Magneto-Responsive Polymers with In-Process Tailorable Composition for Small-Scale Soft Robotics. Adv. Mater. Technol. https://doi.org/10.1002/admt.202400463.

Tafoya, R.R., Secor, E.B., 2020. Understanding and Mitigating Process Drift in Aerosol Jet Printing. Flexible and Printed Electronics 5.
Tait, J.G., Witkowska, E., Hirade, M., Ke, T.H., Malinowski, P.E., Steudel, S., Adachi, C., Heremans, P., 2015. Uniform Aerosol Jet printed polymer lines with 30 μm width for 140 ppi resolution RGB organic light emitting diodes. Org. Electron 22, 40–43. https://doi.org/10.1016/j.orgel.2015.03.034.
Uchiyama, H., Ando, T., Kadota, K., Tozuka, Y., 2021. The formation of an amorphous composite between flavonoid compounds: Enhanced solubility in both oil components and aqueous media. J. Drug. Deliv. Sci. Technol 62. https://doi.org/10.1016/j.jddst.2021.102410.
Vakili, H., Kolakovic, R., Genina, N., Marmion, M., Salo, H., Ihalainen, P., Peltonen, J., Sandler, N., 2015. Hyperspectral imaging in quality control of inkjet printed personalised dosage forms. Int. J. Pharm 483, 244–249. https://doi.org/10.1016/j.ijpharm.2014.12.034.
Varshosaz, J., Ghassami, E., 2015. Enhancement of Dissolution Rate of Fenofibrate By Spray Drying Technique : Comparison of Eudragit E-100 , Solutol ® Hs15 and Hydroxypropyl Cellulose As Carriers 63.
Vialpando, M., Backhuijs, F., Martens, J.A., Van den Mooter, G., 2012. Risk assessment of premature drug release during wet granulation of ordered mesoporous silica loaded with poorly soluble compounds itraconazole, fenofibrate, naproxen, and ibuprofen. Eur. J. Pharm. Biopharm 81, 190–198. https://doi.org/10.1016/j.ejpb.2012.01.012.
Vogt, M., Kunath, K., Dressman, J.B., 2008. Dissolution enhancement of fenofibrate by micronization, cogrinding and spray-drying: Comparison with commercial preparations. Eur. J. Pharm. Biopharm. 68, 283–288. https://doi.org/10.1016/j.ejpb.2007.05.010.
Vuddanda, P.R., Alomari, M., Dodoo, C.C., Trenfield, S.J., Velaga, S., Basit, A.W., Gaisford, S., 2018. Personalisation of warfarin therapy using thermal ink-jet printing. Eur. J. Pharm. Sci. 117, 80–87. https://doi.org/10.1016/j.ejps.2018.02.002.
Ward, A., Walton, K., Box, K., Østergaard, J., Gillie, L.J., Conway, B.R., Asare-Addo, K., 2017. Variable-focus microscopy and UV surface dissolution imaging as complementary techniques in intrinsic dissolution rate determination. Int. J. Pharm 530, 139–144. https://doi.org/10.1016/j.ijpharm.2017.07.053.
Werner, C., Godlinski, D., Zöllmer, V., Busse, M., 2013. Morphological influences on the electrical sintering process of Aerosol Jet and Ink Jet printed silver microstructures. J. Mater. Sci:. Mater. Electron. 24, 4367–4377. https://doi.org/10.1007/s10854-013-1412-y.
Wickström, H., Palo, M., Rijckaert, K., Kolakovic, R., Nyman, J.O., Määttänen, A., Ihalainen, P., Peltonen, J., Genina, N., de Beer, T., Löbmann, K., Rades, T., Sandler, N., 2015. Improvement of dissolution rate of indomethacin by inkjet printing. Eur. J. Pharm. Sci. 75, 91–100. https://doi.org/10.1016/j.ejps.2015.03.009.
Wilkinson, N.J., Smith, M.A.A., Kay, R.W., Harris, R.A., 2019. A review of aerosol jet printing—a non-traditional hybrid process for micro-manufacturing. Int. J. Adv. Manuf. Technol. 105, 4599–4619. https://doi.org/10.1007/s00170-019-03438-2.
Williams, N.X., Watson, N., Joh, D.Y., Chilkoti, A., Franklin, A.D., 2020. Aerosol jet printing of biological inks by ultrasonic delivery. Biofabrication. https://doi.org/10.1088/1758-5090/ab5cf5.
Winter, C., Zettl, M., Mantanus, J., Hadjittofis, E., Leitinger, G., Kolb, D., Hsiao, W.K., Spoerk, M., Paudel, A., Roblegg, E., Pinto, J.T., 2023. Development of a Workflow to Engineer Tailored Microparticles Via Inkjet Printing. Pharm. Res 40, 281–294. https://doi.org/10.1007/s11095-022-03426-4.
Xia, D., Shrestha, N., van de Streek, J., Mu, H., Yang, M., 2016. Spray drying of fenofibrate loaded nanostructured lipid carriers. Asian. J. Pharm. Sci 11, 507–515. https://doi.org/10.1016/j.ajps.2016.01.001.
Xiao, Y., Kalaitzidou, K., Yao, D., Yeo, W., Harris, T.A.L., 2020. Challenges and Advances in Aerosol Jet Printing of Regenerated Silk Fibroin Solutions. Adv. Mater. Interfaces 7. https://doi.org/10.1002/admi.201902005.
Xu, B., Lei, C., Tang, W., Yu, P., Yu, J., Cao, W., 2023. Circulating ink supply system for nozzle array and control method of circulating ink supply system. CN116442654A.
Yang, C., Zhou, E., Miyanishi, S., Hashimoto, K., Tajima, K., 2011. Preparation of Active Layers in Polymer Solar Cells by Aerosol Jet Printing. ACS. Appl. Mater. Interfaces 3, 4053–4058. https://doi.org/10.1021/am200907k.
Yoo, D., Mahoney, C., Deneault, J., Grabowski, C., Austin, D., Berrigan, J., Glavin, N., Buskohl, P., 2021. Mapping drift in morphology and electrical performance in aerosol jet printing. Progr. Additive. Manuf. 6, 1–12. https://doi.org/10.1007/s40964-021-00165-7.
Yousaf, A.M., Kim, D.W., Yong, C.S., Kim, J.O., Choi, H.-G., 2015. Enhanced oral bioavailability of fenofibrate using polymeric nanoparticulated systems : physicochemical characterization and in vivo investigation. Int. J. Nanomedicine 10, 1819–1830.
Yun, Y.H., Kim, J.D., Lee, B.K., Cho, Y.W., Lee, H.Y., 2009. Polymer inkjet printing : construction of three-dimensional structures at micro-scale by repeated lamination. Macromol. Res 17, 197–202.
Zhang, J., Baumberg, J.J., Kar-Narayan, S., 2024. The thickness-dependent response of aerosol-jet-printed ultrathin high-aspect-ratio electrochemical microactuators. Soft. Matter. https://doi.org/10.1039/d4sm00886c.
Zhang, M., Li, H., Lang, B., O'Donnell, K., Zhang, H., Wang, Z., Dong, Y., Wu, C., Williams, R.O., 2012. Formulation and delivery of improved amorphous fenofibrate solid dispersions prepared by thin film freezing. Eur. J. Pharm. Biopharm. 82, 534–544. https://doi.org/10.1016/j.ejpb.2012.06.016.
Zhou, X., Zhang, L., Wang, Y., Zhao, S., Zhou, Y., Guo, Y., Wang, Y., Liang, J., Chen, H., 2023. Aerosol jet printing of multi-dimensional OECT force sensor with high sensitivity and large measuring range. Adv. Mater. Technol 8. https://doi.org/10.1002/admt.202201272.